Characterization of Polymer/TiO2 Photovoltaic Cells by Intensity Modulated Photocurrent Spectroscopy

ARTICLE *in* THE JOURNAL OF PHYSICAL CHEMISTRY C · JANUARY 2009

Impact Factor: 4.77 · DOI: 10.1021/jp8032512

3 AUTHORS, INCLUDING:

Chong Chen
Henan University
30 PUBLICATIONS **259** CITATIONS

SEE PROFILE

Characterization of Polymer/TiO_2 Photovoltaic Cells by Intensity Modulated Photocurrent Spectroscopy

Chong Chen,[†] Mingtai Wang,*[,†,‡] and Kongjia Wang[†]

Institute of Plasma Physics, Chinese Academy of Sciences, Hefei 230031, P. R. China, and Department of Materials Science and Engineering, Anhui Institute of Architecture & Industry, Hefei 230022, P. R. China

Received: April 15, 2008; Revised Manuscript Received: October 27, 2008

A dynamic model for the intensity modulated photocurrent spectroscopy (IMPS) of bilayer polymer/TiO_2 photovoltaic cells is developed in consideration of the exciton generation in the polymer layer, exciton diffusion to the polymer/TiO_2 interface, electron injection into the TiO_2 layer, and electron diffusion through the TiO_2 layer; particularly, the phase shift $\phi_n(\omega)$ due to the time delay between exciton generation and dissociation is included in the continuity equations for electron transport. Bilayer polymer/TiO_2 cells consisting of poly(2-methoxy-5-(2-ethylhexyloxy)-1,4-phenylene vinylene) (MEH-PPV) and nanostructured TiO_2 were prepared for experimental purposes, with a TiO_2 layer thickness d of 120 and 65 nm. Experimental data obtained confirm all the main expectations of the model, providing important information on incident photon-to-current conversion efficiency (IPCE), exciton dissociation, and electron transport. The frequency-dependent $\phi_n(\omega)$ affects the location (P_{high}) where IMPS response crosses with the positive real axis at high frequency, by imposing a $\phi_n(\omega)$ effect on electron transport in the TiO_2 layer to the collection electrode. A more remarkable $\phi_n(\omega)$ effect results from either a larger electron diffusion coefficient D_e in TiO_2 or a smaller d. An increased d value makes the P_{high} point tend toward the origin and the electron transit time τ_D through TiO_2 layer increase, but both S and IPCE values decrease, and the IPCE value depends greatly on the exciton dissociation rate S at the polymer/TiO_2 interface. The measured IMPS responses of the cells are satisfactorily fitted to the model. Dynamic results show that both cells exhibit a $\phi_n(\omega)$ effect with ω_0 of 6×10^4 rad/s and a D_e of 2×10^{-5} cm^2/s, but the different d values lead to varied τ_D, S, and IPCE values, which are, respectively, 1.90 ms, 141 cm^2/s and 0.380% for $d = 120$ nm, but 0.48 ms, 153 cm^2/s, and 0.410% for $d = 65$ nm. Our studies demonstrate that the exciton dissociation efficiency at the polymer/TiO_2 interface is crucially important for highly efficient device performance.

1. Introduction

The motivation for using nanostructured materials to get access to the third generation of photovoltaic (PV) cells emerges from the specific physical and chemical properties of nanostructures.[1,2] Organic PV cells based on conjugated polymers as the donor (D) and nanocrystals as the acceptor (A) are of great interest due to their advantages over conventional Si-based cells, such as low cost, easy processability, and capability to make flexible devices.[3−6] Among the different configurations, the cells with a bilayer structure consisting of donor and acceptor semiconductors are attractive for efficient devices if suitable donor and acceptor materials with complementary electronic and optical properties are developed because photogenerated electrons and holes are, to a great extent, confined to acceptor and donor sides of the D/A interface, respectively. The resulted spatial separation of electrons and holes will minimize the charge recombination and facilitate the transport of charge carriers to the correct electrodes with greatly reduced energy loss at the wrong electrodes.[3−6]

The conversion of light into electricity by an organic PV cell generally involves the following steps: formation of excitons by photon absorption; exciton diffusion to the D/A interface where charge separation occurs; and charge transport within D and A semiconductors to the respective electrodes. Understanding the charge separation and transport is crucially important for the improvement of device performance. Intensity modulated photocurrent spectroscopy (IMPS), a dynamic photoelectrochemical method, has been used as a powerful tool for this purpose,[7−21] in particular, in dye-sensitized solar cells (DSCs).[7−12] The typical DSCs are normally arranged in a sandwich configuration; that is, the space between the dye-sensitized nanoporous TiO_2 and counter electrodes is filled with an organic solution containing the I^-/I^-_3 redox couple as the electrolyte. IMPS measures the periodic photocurrent response to a small sinusoidal perturbation of light, $I_{ac} = I_0\delta e^{i\omega}$, superimposed on a larger steady background level I_0, and provides information about the dynamics of charge transport under short circuit conditions. In the cases of DCSs, the average effective transit time of electrons τ_D in the TiO_2 film[7] can be calculated from the frequency f_{min} value of the lowest imaginary component on a complex plane IMPS plot according to $\tau_D = (2\pi f_{min})^{-1}$, and the real component at a sufficiently low frequency gives a direct estimation of incident photon-to-current conversion efficiency (IPCE) if the photocurrent J_{photo} is divided by the photon flux.[9] However, only a few reports on the IMPS studies of bilayer organic PV cells have been published.[19−21]

For a detailed analysis of charge transport properties, the experimental IMPS response needs a fit to a suitable theoretical model, which strongly correlates to the cell configuration. The bilayer polymer/TiO_2 devices show some similarities to the

* Corresponding author. Tel./Fax: 0086-551-5593171. E-mail address: mtwang@ipp.ac.cn.
† Chinese Academy of Sciences.
‡ Anhui Institute of Architecture & Industry.

10.1021/jp8032512 CCC: $40.75
Published on Web 01/06/2009

typical DSCs with respect to their working principles; that is, the conjugated polymer replaces the dye and electrolyte, bringing together the functions of the sensitizer and hole transporter.[22−25] On the other hand, there are considerable distinctions between these two kinds of devices with respect to the spatial distribution of D/A interfaces. Because of the facts that the phase shift due to the time delay between the exciton generation and the exciton dissociation at the TiO_2/dye interface can be ignored in that the dye molecules assemble on TiO_2 nanoparticle surfaces in a form of monolayer and that the distribution of the D/A interfaces in the nanoporous TiO_2 film is three dimensional, the exciton generation, charge separation, and electron transportation occur three dimensionally and simultaneously within the TiO_2 film in the DSCs, with the presence of a serious recombination between the photogenerated electrons and the electrolyte molecules.[7−12,26,27] However, in the cases of the bilayer polymer/TiO_2 cells, the D/A interface almost only exists near the surface of the TiO_2 film due to the difficult penetration of polymers into the TiO_2 film; the exciton generation occurs mainly in the polymer layer, but the charge separation happens at the D/A interface after a certain time delay (i.e., phase shift) due to the exciton diffusion;[26,27] and the electron transportation proceeds with a strongly minimized charge recombination as a consequence of the spatial separation of electrons and holes.[3−6] With respect to those essential distinctions, therefore, direct application of the IMPS model developed for the DSCs to the bilayer polymer/TiO_2 devices is not plausible. Up to now, no general dynamic IMPS model and analytical solutions for bilayer polymer/TiO_2 devices have been available, and the published IMPS results in bilayer organic PV cells were only modeled using either kinetic equations for minority carrier traps and releases[19] or equivalent circuit method[20] or were analyzed by a phenomenological equation for the *ac* photocurrent.[21] In this paper, we develop an IMPS model for bilayer polymer/TiO_2 cells, and attention is given to the exciton generation in the polymer layer, the exciton diffusion to the D/A interface, the injection of separated electrons into TiO_2 film, and the diffusion of electrons through the TiO_2 layer to back contact; the experimental IMPS responses of bilayer polymer/TiO_2 cells are measured and well fitted to the analytical expressions of our model, providing new insights into the electron transport in such devices.

2. Experimental Section

Poly(2-methoxy-5-(2-ethylhexyloxy)-1,4-phenylenevinylene) (MEH-PPV) (Avg. M_n = 40 000−70 000) was purchased from Aldrich. Titanium tetraisopropoxide [$Ti(O^iPr)_4$] (Acros, 98+%) was used as TiO_2 precursor. The bilayer PV devices, with a structure of ITO/TiO_2/MEH-PPV/Au as shown in Figure 1a, were constructed by spinning down first a nanostructured titanium dioxide (TiO_2) layer and then a MEH-PPV layer over indium tin oxide (ITO, ≤15 Ω/□, Wuhu Token Sci. Co., Ltd., China) sheet glass, as described elsewhere.[22] The TiO_2 sol−gel was prepared from a mixture of titanium tetraisopropoxide, absolute ethanol, and acetic acid (GR, ≥99.8%), in a volume ratio of *w*:20:0.1. The mixture was stirred at room temperature until a homogeneous colorless stable TiO_2 sol was obtained. An etched ITO substrate was spin-coated with the TiO_2 sol at 2500 rpm for 40 s in ambient conditions. The freshly coated TiO_2 film was exposed to a humid air (50% relative humidity) overnight, in order to get a full hydrolysis of the precursor and a good polymerization of the Ti−O network. Then the TiO_2 film was sintered in a tube furnace under a nitrogen trickle. The temperature of the furnace was slowly raised at a rate of 1 °C/min up to 550 °C and held at this temperature for 30 min and then cooled at a rate of 1 °C/min to room temperature. The preparation procedure produced the TiO_2 films of 65 (w = 2) and 120 (w = 5) nm in thickness.

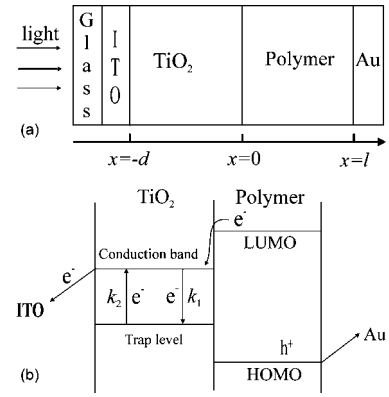

Figure 1. Geometry of the bilayered device under illumination (a) and the steps involved in transport of injected electrons (b). The coordinates $x = -d$, 0, and l indicate the ITO/TiO_2 interface, the D/A interface, and the polymer/Au interface, respectively. Rate constants k_1 and k_2 are for trapping and detrapping, respectively. The HOMO and LUMO indicate the highest occupied molecular orbital and lowest unoccupied molecular orbital energy levels of polymer, respectively.

A thin MEH-PPV layer of 220 nm in thickness was spin-coated (3000 rpm, 40 s) onto the TiO_2 layer in ambient conditions from a solution (16 mg/mL) in freshly dried THF. Then, a gold back contact layer (100 nm) was deposited by thermal evaporation onto the MEH-PPV layer from a gold wire (99.999%) of 1 mm diameter at an initial deposition rate of 0.2 nm/s that was raised to 0.9 nm/s at the end of deposition. The cell devices were sealed in a glovebox (O_2 < 0.5 ppm, H_2O < 3 ppm), and silver paste was used to create external contacts.

The thickness of TiO_2 and MEH-PPV films was measured by field-emission scanning electron microscopy (FESEM, FEI Sirion 200). Steady-state current−voltage ($J-V$) characteristics and the IMPS spectra were measured on a controlled intensity modulated photo spectroscopy (CIMPS) (Zahner Co., Germany) in ambient conditions under illumination through the ITO glass side, using a blue light-emitting diode (LED) as the light source (BLL01, λ_{max}= 470 nm, spectral half-width = 25 nm, Zahner Co.) driven by a frequency response analyzer, and the light intensity of the *dc* component (15.85 mW/cm^2) was controlled by the bias voltage at the LED with a proportionality factor FP = 135.7 W·m^{-2}·V^{-1} that was calibrated using an IL1400A photometer with a SEL 033/W detector (International Light, Inc., USA). $J-V$ characteristics were recorded within the bias voltage range of −1 to +1 V with a voltage increment of 0.01 V. In the IMPS measurements, the small sinusoidal perturbation $I_{ac}= I_0\delta e^{i\omega t}$ (1.54 mW/cm^2) was used, about a depth δ = 10% of the *dc* light intensity. During the steady-state measurements, the gold and ITO contacts were taken as negative and positive electrodes, respectively, while the electrodes were reversed in the dynamic measurements. For all measurements, the effective illumination area of the cells was 0.16 cm^2.

3. IMPS Model

The interfacial processes involved in charge transportation in the polymer/TiO_2 cells are depicted by Figure 1b. As exciton dissociation occurs, transport of the free charge carriers to the electrodes can be by diffusion alone[26] or may be assisted by a built-in electric field provided by a difference between the electrode work functions.[27−29] Since the drift rate of electrons in TiO_2 due to the built-in electric field is at least an order of

magnitude lower than their diffusion rate[28] and the electric field is usually not strong enough to cause the exciton dissociation,[26,27] we ignore the electric field influences to simplify our model. Additionally, the following assumptions are given: (1) photoexcitation produces excitons only in the polymer layer, only exciton dissociation at the D/A interface contributes to the photocurrent,[30,31] and the possible intrinsic dissociation in the bulk polymer is negligible;[32] (2) since the diffusion transport of electrons injected into the TiO_2 film is strongly influenced by trapping and detrapping effects,[7,13−15] the electronic transport in the nanocrystalline TiO_2 layer is controlled only by trapping and detrapping processes in the band gap; and (3) the holes remaining in the polymer recombine fast with the electrons from the external circuit under the short circuit; i.e., the holes do not contribute to photocurrent.

As is well-known, the exciton transport in conjugated polymers under steady-state conditions can be described by the standard diffusion equation.[32−38] If the time-dependent density of photogenerated excitons at the location x away from the D/A interface where $x = 0$ (Figure 1a) is $p(x,t)$ and the mean exciton lifetime is τ_p, the continuity equation for the exciton density in the polymer layer can be written as

$$\frac{\partial p(x,t)}{\partial t} = \theta\alpha_p I_0 e^{-\alpha_p x} + D_p\frac{\partial^2 p(x,t)}{\partial x^2} - \frac{p(x,t)}{\tau_p} \quad (1)$$

where θ is the quantum efficiency of exciton generation by light absorption; α_p is the absorption coefficient of polymer as a function of photon wavelength λ; D_p the diffusion coefficient of excitons; and I_0 is the incident light intensity.

In IMPS, the modulated illumination consists of a *dc* component of a steady-state bias light intensity I_0 (i.e., photon flux per m^2) and an *ac* component of a small sinusoidal perturbation $I_{ac} = I_0\delta e^{i\omega t}$. The periodic illumination function is described as $I(x,t) = I_0(1 + \delta e^{i\omega t})$, where $\omega = 2\pi f$ is the variable modulation frequency and $\delta \ll 1$ in order to allow the linearization of the system response.[11,16] The continuity equation for the position- and time-dependent density $p(x,t)$ of photogenerated excitons in the polymer layer under the modulated illumination is then written as[32−38]

$$\frac{\partial p(x,t)}{\partial t} = \theta I(x,t)\alpha_p e^{-\alpha_p x} + D_p\frac{\partial^2 p(x,t)}{\partial x^2} - \frac{p(x,t)}{\tau_p} \quad (2)$$

Under the modulated illumination, the exciton density can be written as $p(x,t) = p_0(x) + \Delta p(x)e^{i\omega t}$, where $p_0(x)$ is the steady-state exciton density, and independent of time, $p_{ac}(x,t) = \Delta p(x)e^{i\omega t}$ represents the *ac* component of exciton density. The following expression is derived from eq 2

$$\frac{\partial^2 \Delta p(x)}{\partial x^2} = \gamma^2 \Delta p(x) - \frac{\theta\alpha_p I_0 \delta}{D_p} e^{-\alpha_p x} \quad (3)$$

with

$$\gamma = \sqrt{\frac{1}{D_p\tau_p} + \frac{i\omega}{D_p}} \quad (4)$$

The interfacial dissociation of photogenerated excitons is crucially important for the photovoltaic effect.[3−6,30,31] The exciton at a D/A interface will decay into the ground state or dissociate into free charge carriers, and the separation into the free charge carriers is a competition between dissociation and recombination.[39,40] However, the kinetics of exciton dissociation at the D/A interface is complicated and not well understood.[26,27,41] Many factors may impact the dissociation process, such as the thickness of the polymer layer,[33,38,41] the exciton[42] and electron[43] diffusion coefficients, and the charge recombination rate at the D/A interface.[44] For simplicity, we assume that the excitons dissociate at the D/A interface with a constant rate S (cm/s), similar to the quenching velocity of excitons at an interface,[33] and the detailed kinetics of the dissociation is not considered to impact the charge transportation dynamics. Moreover, it is taken that there exist no excitons at the polymer/metal interface ($x = l$) due to dissociation or recombination.[37] Hence, two boundary conditions are obtained as

$$D_p\frac{\partial \Delta p(x)}{\partial x}\bigg|_{x=0} = S\Delta p(0) \quad (5)$$

and

$$\Delta p(l) = 0 \quad (6)$$

where l is the polymer film thickness, and $S\Delta p(0)$ represents the annihilation flux density of excitons at the D/A interface. With the above boundary conditions, the solution of eq 3 can be described by

$$\Delta p(x) = Ae^{\gamma x} + Be^{-\gamma x} + Ce^{-\alpha_p x} \quad (7)$$

with

$$A = \frac{-Be^{-\gamma l} - Ce^{-\alpha_p l}}{e^{\gamma l}} \quad (8)$$

$$B = \frac{\left(\frac{S}{D_p} - \gamma\right)e^{-\alpha_p l} - \left(\alpha_p + \frac{S}{D_p}\right)e^{\gamma l}}{\left(\frac{S}{D_p} + \gamma\right)e^{\gamma l} + \left(\gamma - \frac{S}{D_p}\right)e^{-\gamma l}} C \quad (9)$$

$$C = \frac{\theta\alpha_p\delta I_0}{D_p(\gamma^2 - \alpha_p^2)} \quad (10)$$

On the other hand, the excess electron densities in the conduction band of TiO_2 [i.e., $n(x,t)$] and in the trap states [i.e., $N(x,t)$] (Figure 1b) are described by the following continuity equations[7,14,15,45]

$$\frac{\partial n(x,t)}{\partial t} = D_e\frac{\partial^2 n(x,t)}{\partial x^2} - k_1 n(x,t) + k_2 N(x,t) - \frac{n(x,t)}{\tau_e} \quad (11)$$

$$\frac{\partial N(x,t)}{\partial t} = -k_2 N(x,t) + k_1 n(x,t) \quad (12)$$

where τ_e is the electron lifetime in the conduction band and $D_e = D_{cb}k_2/k_1$ is the effective diffusion coefficient of electrons with D_{cb} being the diffusion coefficient of electrons in the conduction band.[10] k_1 and k_2 are the first-order rate constants for trapping and detrapping, respectively. Since the polymer layer is normally much thicker than a monolayer in practical devices, there, due to exciton diffusion in polymer,[26,27] will be a remarkable time delay between the photo excitation in the polymer and electron generation at the D/A interface, which is rather different from the typical DSCs where this delay can be ignored[7−12,26,27] (refer to Introduction). The time delay will manifest itself as a frequency-dependent phase shift in IMPS response, as is similar to the case of electron diffusion in TiO_2.[8,12] Therefore, two electron densities can be expressed as

$$n(x,t) = n_0(x) + \Delta n(x)e^{i[\omega t - \phi_n(\omega)]} \quad (13)$$

$$N(x,t) = N_0(x) + \Delta N(x)e^{i[\omega t - \phi_N(\omega)]} \quad (14)$$

where the first terms on the right of eqs 13 and 14 are the steady-state electron densities, and the second terms are the *ac* components of electron densities; $\phi_n(\omega)$ and $\phi_N(\omega)$ are the

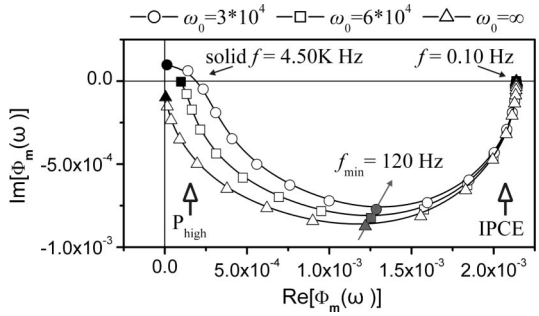

Figure 2. Dependence of the calculated IMPS responses upon the parameter ω_0. The parameters for calculation are $d = 100$ nm, $l = 220$ nm, $D_e = 5 \times 10^{-5}$ cm^2/s, $S = 80$ cm/s, $\alpha_p = 10^5$ cm^{-1}, $k_1 = 8 \times 10^5$ s^{-1}, $k_2 = 1.0 \times 10^3$ s^{-1}, $D_p = 3 \times 10^{-3}$ cm^2/s, $\tau_p = 300 \times 10^{-12}$ s, $k_{ext} = \infty$, $\tau_e = 0.01$ s, $R = 20\ \Omega$, $C = 2 \times 10^{-5}$ F.

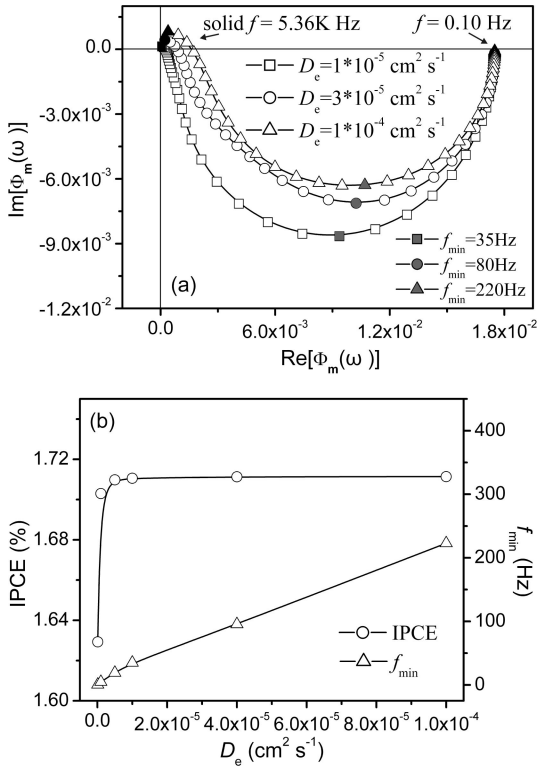

Figure 3. Dependence of the calculated (a) IMPS responses and (b) values of IPCE and f_{min} upon D_e, with $S = 800$ cm/s and $\omega_0 = 4 \times 10^4$ rad/s. Other parameters for calculation are the same as those in Figure 2.

frequency-dependent phase shifts, which are due to the magnification of the time delay between the exciton densities at the generation position and the D/A interface; and the term of $[\omega t - \phi_n(\omega)]$ represents the total phase shift between the photogenerated exciton density and the electron density at position x ($-d \le x \le 0$). On one hand, as described above, the phase shift $\phi_n(\omega)$ is dependent on the modulation frequency ω. On the other hand, if the frequency approaches zero (i.e., $\omega \rightarrow 0$), namely, under a steady-state illumination, there is no phase difference between the exciton densities at the generation position and D/A interface [i.e., $\phi_n(\omega) \rightarrow 0$]. With these considerations, we simply define $\phi_n(\omega) = \pi\omega/\omega_0$ in our model, with ω_0 (rad/s) to be a constant depending on the intrinsic property of the conjugated polymer. Hence, the continuity equation for the electron density $\Delta n(x)$ in the conduction band is expressed as

$$\frac{\partial^2 \Delta n(x)}{\partial x^2} = \beta^2 \Delta n(x) \tag{15}$$

with

$$\beta = \sqrt{\frac{-\omega^2 + i(k_1 + k_2)\omega}{D_e(k_2 + i\omega)} + \frac{1}{D_e \tau_e}} \tag{16}$$

Since the electron density at the polymer/TiO_2 interface ($x = 0$) is determined by the S and correlated with the phase shift $\phi_n(\omega)$ and if the extraction of electrons from TiO_2 to the ITO substrate at the ITO/TiO_2 interface ($x = -d$) is assumed to proceed with a rate constant k_{ext}, then two boundary conditions for eq 15 are given by

$$D_e \frac{\partial \Delta n(x)}{\partial x}\bigg|_{x=0} = S\Delta p(0) e^{i\phi_n(\omega)} \tag{17}$$

$$D_e \frac{\partial \Delta n(x)}{\partial x}\bigg|_{x=-d} = k_{ext} \Delta n(-d) \tag{18}$$

Using the above conditions, the solution of eq 15 is derived as

$$\Delta n(x) = c_1 e^{-\beta x} + c_2 e^{\beta x} \tag{19}$$

with coefficients c_1 and c_2 to be

$$c_1 = \frac{S\Delta p(0)}{D_e \beta} \frac{\left(1 - \frac{k_{ext}}{D_e \beta}\right) e^{-\beta d + i\phi_n(\omega)}}{\left(1 + \frac{k_{ext}}{D_e \beta}\right) e^{\beta d} + \left(\frac{k_{ext}}{D_e \beta} - 1\right) e^{-\beta d}} \tag{20}$$

$$c_2 = \frac{S\Delta p(0) e^{i\phi_n(\omega)}}{D_e \beta} + c_1 \tag{21}$$

The solution for the diffusion-limited short circuit can be obtained for a large enough k_{ext} value from eq 19, and the *ac* component of the photocurrent is given by

$$\Delta j(\omega) = q D_e \frac{\partial \Delta n(x)}{\partial x}\bigg|_{x=-d} \tag{22}$$

where q is the elementary charge. The *ac* photocurrent conversion efficiency $\varphi(\omega) = \Delta j(\omega)/q\delta\theta I_0$. As shown in the DSCs,[7,12] the experimentally measured IMPS response is often affected by *RC* attenuation of the electrode, especially toward higher frequencies. In general, to include the *RC* attenuation, the measured IMPS response Φ_m is obtained by multiplying $\varphi(\omega)$ with the complex attenuation function $F(\omega) = (1 + i\omega RC)^{-1}$; that is, $\Phi_m(\omega) = \varphi(\omega)F(\omega)$. Thus

$$\Phi_m(\omega) = \frac{2k_{ext} S\Delta p(0) e^{i\phi_n(\omega)}}{\delta\theta I_0 [(D_e\beta + k_{ext}) e^{\beta d} + (k_{ext} - D_e\beta) e^{-\beta d}]} \cdot \frac{1}{1 + i\omega RC} \tag{23}$$

R is the series resistance, and C is the capacitance of the electrode. Under short circuit conditions, R and C are mainly due to the conducting glass substrate, with the typical values of around 10−20 Ω and 30 μF for the ITO substrate.[7,9,12]

The dependence of the IMPS responses calculated from eq 23 on different parameters is shown in Figures 2 to 5. During our calculations, $\theta = 1$ and $k_{ext} = \infty$ were given, and we took $\tau_p = 300$ ps[23,46] and $\alpha_p(\lambda = 470\ \text{nm}) = 10^5$ cm^{-1} for MEH-PPV. Assuming a three-dimensional random walk of the excitons in the polymer film, the exciton diffusion coefficient of $D_p = 3 \times 10^{-3}$ cm^2/s was obtained according to $D_P = L_p^2/6\tau_p$ with exciton diffusion length $L_P = 20$ nm.[23] Moreover, because of no or very weak recombination of excess electrons

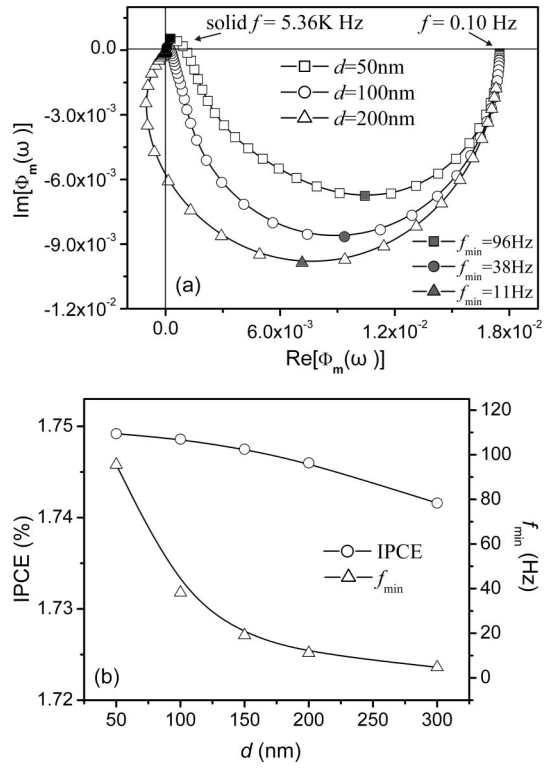

Figure 4. Dependence of the calculated (a) IMPS responses and (b) values of IPCE and f_{min} on d, with $D_e = 1 \times 10^{-5}$cm^2/s, $S = 800$ cm/s and $\omega_0 = 4 \times 10^4$ rad/s. Other parameters for calculation are the same as those in Figure 2.

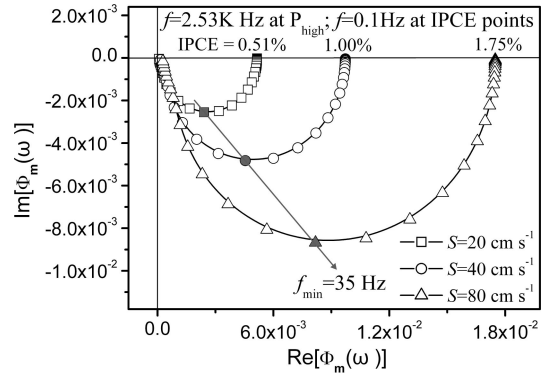

Figure 5. Dependence of the calculated IMPS responses upon S, with $D_e = 1 \times 10^{-5}$ cm^2/s and $\omega_0 = 4 \times 10^4$ rad/s. Other parameters for calculation are the same as those in Figure 2.

in the conduction band and trapped states, we took $\tau_e = 0.01$ s for calculations, by referring to that in DSCs where τ_e is normally $\approx 10^{-3} \sim 10^{-2}$ s depending on incident light intensity.[7,9,47]

4. Results and Discussion

The calculated IMPS responses appear mainly in the fourth quadrant (positive real, negative imaginary) of the complex plane as the result of the time delay between electron injection and collection, which is similar to the cases of DSCs.[7−12] As shown in Figure 2, however, the IMPS response crosses the positive real axis from the fourth quadrant into the first quadrant of the complex plane at high frequencies when the phase shift $\phi_n(\omega)$ exists. For a convenient discussion, we refer the crossing points of an IMPS response with the positive real axis at high and low frequencies to P_{high} and IPCE points (indicated by the arrows in the low part of the plot in Figure 2), respectively. Increasing ω_0 makes the P_{high} point tend to the origin. Particularly, in the limit $\omega_0 \rightarrow \infty$ (i.e., the effect of $\phi_n(\omega)$ is negligible), the IMPS plot spirals into the origin, as is similar to the cases of DSCs in which the phase shift $\phi_n(\omega)$ can be ignored.[7−12,26,27] When changing ω_0, no obvious influences imposed by $\phi_n(\omega)$ on the location of the IPCE point and the f_{min} value of the lowest imaginary component were found (Figure 2).

Figure 3 shows the dependence of IMPS responses on the electron diffusion coefficient D_e. With decreasing D_e value (Figure 3a), the P_{high} point of the IMPS response tends toward the origin, which is similar to the case of the enhanced ω_0 (Figure 2), but the f_{min} value decreases. Further calculations show that D_e imposes a remarkable influence on the f_{min} value, but rather a faint effect on the location of the IPCE point (Figure 3b). As for a given polymer layer, $\phi_n(\omega)$ is equal for the cases of different D_e values: a larger D_e will lead to a more obvious $\phi_n(\omega)$ effect on the electron transport through the TiO_2 film to the collection electrode via decreasing transit time τ_D [$= (2\pi f_{min})^{-1}$], as compared to the case of a smaller D_e, especially at high frequencies. Therefore, the D_e dependence of the location of the P_{high} point originates actually from the total phase shift $[\omega t - \phi_n(\omega)]$ that is changed by the electron diffusion kinetics.

With increasing the thickness d of the TiO_2 layer, the f_{min} value decreases and the P_{high} point tends to pass through the origin, indicating a bigger $\phi_n(\omega)$ effect on the electron transport in a thinner TiO_2 layer (Figure 4a). However, the IPCE point is hardly changed by d values (Figure 4b). The smaller d value of TiO_2 film inevitably reduces the electron transit time τ_D (Figure 4b), which will cause a more evident $\phi_n(\omega)$ effect on the total phase shift between the electron generation and collection. As d increases up to 200 nm, the calculated IMPS response first loops into the third quadrant (negative real + negative imaginary) before spiraling into the origin (Figure 4a). Such a change in the shape of IMPS response was also observed in DSCs that had either a dye-free TiO_2 layer existing between the electrode substrate and dye-sensitized TiO_2 layer[12] or a TiO_2 layer with different thermal histories on the electrode substrate.[9] The main reason for the shape change is due to the distinct *RC* attenuation as transit time τ_D becomes longer.[7,9,12] Our experimental results also indicate that different d values result in different *RC* effects (refer to Figures 6 and 7).

Different from the parameters ω_0, D_e, and d, which mainly influence the location of the P_{high} point and the f_{min} value of IMPS response, the exciton dissociation rate S at the D/A interface only changes greatly the location of the IPCE point (Figure 5), and a higher S leads to a higher IPCE of the device. Note that the P_{high}points in the calculated IMPS responses in Figure 5 are close to the origin, which is not in contradiction with the demonstration by Figure 2, because the calculation parameter D_e is five times lower than that for Figure 2, resulting in a much smaller $\phi_n(\omega)$ effect on the electron transport (Figure 3).

In short, the above calculations mainly show the influence of the parameter ω_0, D_e, d, and S on the shape of the IMPS response. On one hand, smaller ω_0, smaller d, and larger D_e values produce a more remarkable effect of the phase shift $\phi_n(\omega)$ between the exciton generation and dissociation on the electron transport, leading to the bias of the P_{high} point of IMPS response away from the origin; on the other hand, larger d and smaller D_e result in a smaller f_{min}, indicating a longer transit time τ_D. Both ω_0 and S do not impose obvious influences on the f_{min} value. The IPCE value is sensitive to S value (Figure 5) but not sensitive to other parameters (Figures 2−5), indicating that the dissociation rate S at the D/A interface determines the IPCE

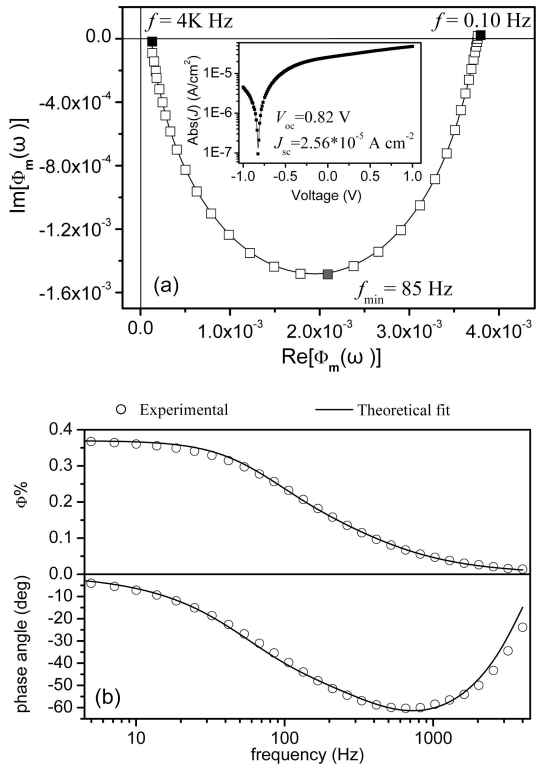

Figure 6. (a) Measured IMPS response in a complex plane for the cell with $d = 120$ nm and $l = 220$ nm. The inset to (a) shows the steady-state current−voltage characteristics of the cell under the *dc* light intensity. (b) The measured and fitted IMPS responses in the form of Bode plot, with fitting parameters: $k_1 = 3.0 \times 10^5$ s^{-1}, $k_2 = 8.5 \times 10^2$ s^{-1}, $D_e = 2 \times 10^{-5}$ cm^2/s, $R = 30$ Ω, $C = 18$ μF, $S = 141$ cm/s, and $\omega_0 = 6 \times 10^4$ rad/s.

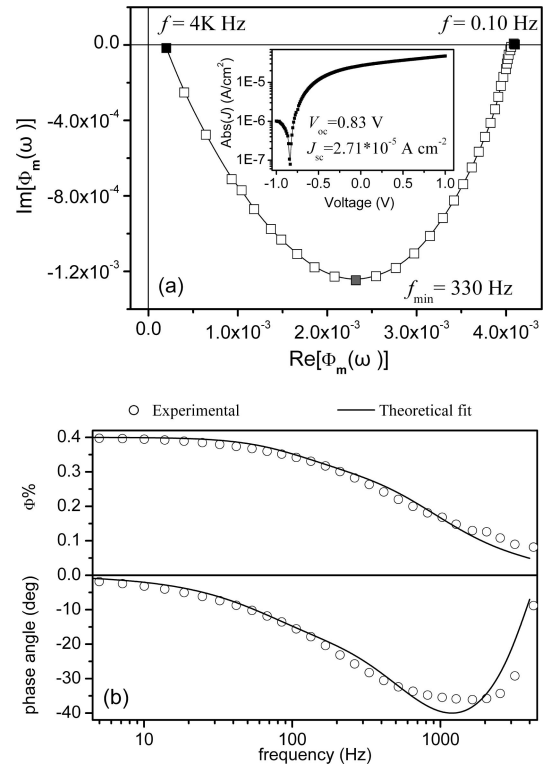

Figure 7. (a) Measured IMPS response in a complex plane for the cell with $d = 65$ nm and $l = 220$ nm. The inset to (a) shows the steady-state current−voltage characteristics of the cell under the *dc* light intensity. (b) The measured and fitted IMPS responses in the form of Bode plot, with fitting parameters: $k_1 = 3.0 \times 10^5$ s^{-1}, $k_2 = 8.5 \times 10^2$ s^{-1}, $D_e = 2 \times 10^{-5}$ cm^2/s, $R = 30$ Ω, $C = 8$ μF, $S = 153$ cm/s, and $\omega_0 = 6 \times 10^4$ rad/s.

value and a higher S value leads to a higher energy conversion efficiency of the device.

Two bilayer devices of ITO/TiO_2/MEH-PPV/Au (Figure 1a) with $d = 120$ and 65 nm ($l = 220$ nm in both cells) were constructed for experiments. Steady-state $J-V$ measurements clearly showed that these devices exhibited an open circuit voltage (V_{oc}) around 0.8 V (insets to Figures 6a and 7a) and a short circuit current J_{sc} of 25.6 ($d = 120$ nm) and 27.1 ($d = 65$ nm) μA/cm^2. Normally, the devices with the configuration as shown in Figure 1a produce open circuit voltages ranging from 0.7 to 1.1 V.[24,25] The J_{sc} values obtained in our cases are about half of those obtained by others in the similar but much smaller cells ($d = 75$ nm, $l = 200$ nm, effective illumination area = 3 mm^2).[24]

The measured IMPS responses are shown in Figures 6a and 7a. The IMPS responses appear in the fourth quadrant, as consistent with the calculated plots according to the model. The IMPS measurements showed that the location of the P_{high} points in the measured IMPS plots were 0.13×10^{-3} for $d = 120$ nm and 0.19×10^{-3} for $d = 65$ nm and that the f_{min} values were 85 Hz (i.e., $\tau_D = 1.90$ ms) for $d = 120$ nm and 330 Hz (i.e., $\tau_D = 0.48$ ms) for $d = 65$ nm. These results are in a good agreement with the theoretical expectation that a larger d makes the P_{high} point tend toward the origin and the electron transit time τ_D increase (Figure 4). The measured IMPS responses (Figures 6a and 7a) cross the positive real axis from the fourth quadrant into the first quadrant of the complex plane at high frequencies before reaching the origin, indicating the presence of a serious phase shift $\phi_n(\omega)$ in both cases.

Since the real component at the sufficiently low frequency on the complex plane IMPS plot gives a direct estimation of IPCE (refer to Introduction and ref 9) and the IPCE value is only sensitive to S (Figures 2−5), the S value is easily estimated using the IPCE value from the measured IMPS response according to eq 23; on the other hand, the ω_0 value can be evaluated from the P_{high} point of the measured IMPS response using eq 23. Therefore, the parameter that needs to be obtained by curve fitting is D_e. First, taking the order of magnitude of 10^{-2} cm^2/s for D_{cb}[10] and that of 10^5 s^{-1} for k_1 with $k_1 > k_2$, then the D_e value was obtained by the best fit with regard to the f_{min} value, that is, by inserting the parameters α_p, D_p, τ_p, l, d, τ_e, ω_0, and S into eq 23 and a simultaneous varying D_e, R, and C until a good accordance with the experimental value of f_{min} was gotten. The Bode plots of the measured IMPS responses were satisfactorily fitted to eq 23 over the whole frequency range by considering the phase shift $\phi_n(\omega)$, as shown in Figures 6b and 7b. During our calculations, the energy loss caused by the conductive substrate was ignored. In order to evaluate the influence of phase shift $\phi_n(\omega)$, the fits were made by keeping $\omega_0 = \infty$ and simultaneously varying D_n, R, and C values. The absence of $\phi_n(\omega)$ could not produce good fits. Figure 8 illustrates an example for the fits by inserting $\omega_0 = \infty$ and the other parameters the same as Figures 6b and 7b. Even though the photocurrent plots are not affected when $\omega_0 = \infty$, the significant deviations occur at higher frequencies with the fitted phase angles approach −90° in the phase plots, indicating that the responses nearly cross the imaginary axis at high frequencies,[7] which differs from the experimental observations. Note, comparing Figures 6b with 7b shows a bit larger deviation between the experimental and calculated data at high frequencies in the case of a thinner TiO_2 layer ($d = 65$ nm), which might be due to the enhanced $\phi_n(\omega)$ phase shift effect and the varied RC

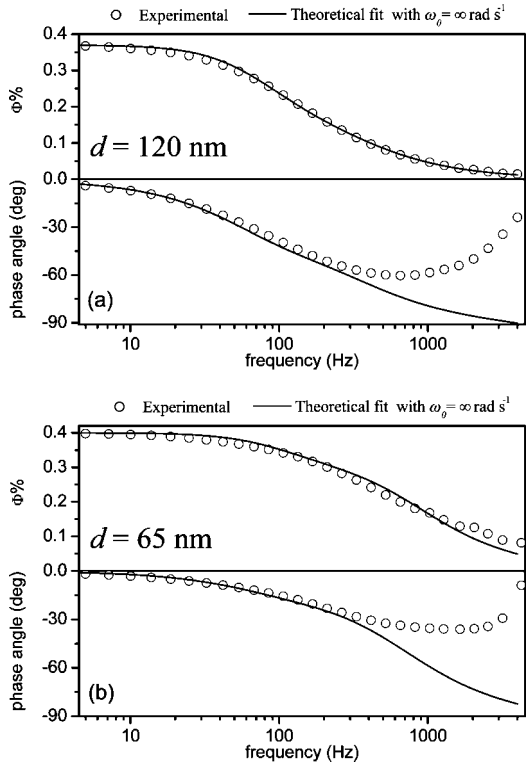

Figure 8. Measured IMPS responses of the cells in Figures 6 and 7 were fitted without consideration of the phase shift $\phi_n(\omega)$. (a) The cell with $d = 120$ nm, and (b) for $d = 65$ nm. During calculations, the parameter ω_0 was set to be $\omega_0 = \infty$, and the other parameters were kept the same as those in Figures 6b and 7b, respectively.

influence, resulting from the thinner TiO_2 thickness, on the electron transport dynamics. This deviation is actually rather small and will not alter the validity of the model for the observed IMPS responses.[7,9,17,18]

The satisfactory fits (Figures 6b and 7b) gave the values of 30 Ω for R and 8, 18 μF for C, which agree with the findings by others.[7,9,12] The electron diffusion coefficient D_e in our cases is of the same order of magnitude as the value obtained in the nanoporous TiO_2 films in DSCs.[7,12] The IPCE values obtained from the dynamic measurements are 0.380% for $d = 120$ nm and 0.410% for $d = 65$ nm, and they are close to the data obtained from steady-state $J-V$ measurements, that is, 0.426% ($d = 120$ nm) and 0.451% ($d = 65$ nm). The result that an increasing IPCE is accompanied with the decrease in the TiO_2 film thickness is consistent with other reports.[22] The S values for d of 120 and 65 nm were calculated from the measured IMPS responses on the basis of our model to be 141 and 153 cm/s, respectively (Figures 6b and 7b), which verifies the model expectation that a higher S will result in a higher IPCE. The values of S obtained by our model are close to the quenching velocity (144 cm/s) of the excitons produced in perylene bis(phenethylimide) (PPEI) at the interfaces between PPEI and nonquenching substrates but much smaller than the exciton quenching velocity of ca. 10^6 at the interfaces between PPEI and quenching substrates.[33] Therefore, the normally low IPCE of bilayer MEH-PPV/TiO_2 cells at the maximum absorption of the polymer (ca. 1−6%)[22,24,25] is very likely due to a rather low exciton dissociation efficiency at the D/A interface, even though previous results indicated that other factors may also be responsible for the low efficiency of organic solar cells.[21] From our simulations (Figures 6 and 7), a higher S value is obtained for a smaller d, but the reason for this phenomenon is not clear from the present model. This may be due to the simplified assumptions that ignore the kinetics of exciton dissociation and the electric field effect on electron transport. As described when introducing the parameter S to our model, the kinetics of exciton dissociation at the D/A interface is related to many factors[33,38,41−44] Besides those factors, the accumulation of charge carriers in D and A layers[19,48−50] will impede the flow of carriers across the D/A interface. Here we speculate a tentative explanation to the d-dependence of S value as follows: as the TiO_2 thickness d increases, more electrons will be trapped and a more serious accumulation of electrons in the TiO_2 layer might occur to impede the charge travel away from the interface and consequently reduce the S value. Finally, it should be noted that, even though the simplified assumptions are made, our model captures most of the salient features of charge carrier transport, and the experimental data confirm all the main predictions of the model. These results give the information on the characteristics of bilayer polymer/TiO_2 devices.

5. Conclusions

This study presents a dynamic IMPS model for the bilayer polymer/TiO_2 photovoltaic cells, on the basis of the continuity equations for excess exciton density in the polymer and electron density in the conduction band of TiO_2, particularly in consideration of the frequency-dependent phase shift $\phi_n(\omega)$ due to the time delay between exciton generation and dissociation. The experimental data obtained from bilayer MEH-PPV/TiO_2 cells confirm all the main predictions of the model, providing information on the IPCE value and the characteristics [$\phi_n(\omega)$, S, and D_e] of the exciton dissociation and electron transport. The phase shift $\phi_n(\omega)$ affects the location (P_{high}) where IMPS response crosses with the positive real axis at high frequency, by imposing an effect on electron transport through the TiO_2 layer to the collection electrode. A more remarkable $\phi_n(\omega)$ effect results from either a larger electron diffusion coefficient D_e in TiO_2 or a smaller TiO_2 thickness d. An increased d value makes the P_{high} point tend toward the origin, the electron transit time τ_D through the TiO_2 layer increase, and both S and IPCE values decrease. The IPCE of the bilayer cells depends greatly on the exciton dissociation rate S at the polymer/TiO_2 interface. A rather low exciton dissociation efficiency at the D/A interface should be responsible for the normally low IPCE values of the MEH-PPV/TiO_2 cells reported,[22,24,25] and the enhancement of the dissociation efficiency will be crucially important for highly efficient device performance.

Acknowledgment. This work was supported by the "100-talent Program" of Chinese Academy of Sciences, the Scientific Research Foundation for the Returned Overseas Chinese Scholars, State Education Ministry, and the National Natural Science Foundation of China (No. 20474066). We also acknowledge the referees involved for their generous advice on revision.

References and Notes

(1) Catchpole, K. R. *Phil. Trans. R. Soc. A* **2006**, *364*, 3493–3503.
(2) Conibeer, G.; Green, M.; Corkish, R.; Cho, Y.; Cho, E.-C.; Jiang, C.-W.; Fangsuwannarak, T.; Pink, E.; Huang, Y.; Puzzer, T.; Trupke, T.; Richards, B.; Shalav, A.; Lin, K.-L. *Thin Solid Films* **2006**, *511−512*, 654–662.
(3) Coakley, K. M.; McGehee, M. D. *Chem. Mater.* **2004**, *16*, 4533–4542.
(4) Benanti, T. L.; Venkataraman, D. *Photosynth. Res.* **2006**, *87*, 73–81.
(5) Gledhill, S. E.; Scott, B.; Gregg, B. A. *J. Mater. Res.* **2005**, *20*, 3167–3179.
(6) Günes, S.; Neugebauer, H.; Sariciftci, N. S. *Chem. Rev.* **2007**, *107*, 1324–1338.

(7) Dloczik, L.; Ileperuma, O.; Lauermann, I.; Peter, L. M.; Ponomarev, E. A.; Redmond, G.; Shaw, N. J.; Uhlendorf, I. *J. Phys. Chem. B* **1997**, *101*, 10281–10289.
(8) Krüger, J.; Plass, R.; Grätzel, M.; Cameron, P. J.; Peter, L. M. *J. Phys. Chem. B.* **2003**, *107*, 7536–753.
(9) Oekermann, T.; Zhang, D.; Yoshida, T.; Minoura, H. *J. Phys. Chem. B* **2004**, *108*, 2227–2235.
(10) Fisher, A. C.; Peter, L. M.; Ponomarev, E. A.; Walker, A. B.; Wijayantha, K. G. U. *J. Phys. Chem. B* **2000**, *104*, 949–958.
(11) Peter, L. M.; Wijayantha, K. G. U. *Electrochem. Commun.* **1999**, *1*, 576–580.
(12) Franco, G.; Peter, L. M.; Ponomarev, E. A. *Electrochem. Commun.* **1999**, *1*, 61–64.
(13) de Jongh, P. E.; Vanmaekelbergh, D. *Phys. Rev. Lett.* **1996**, *77*, 3427–3430.
(14) de Jongh, P. E.; Vanmaekelbergh, D. *J. Phys. Chem. B* **1997**, *101*, 2716–2722.
(15) Vanmaekelbergh, D.; de Jongh, P. E. *Phys. Rev. B* **2000**, *61*, 4699–4704.
(16) Peter, L. M. *Chem. Rev.* **1990**, *90*, 753–769.
(17) Franco, G.; Gehring, J.; Peter, L. M.; Ponomarev, E. A.; Uhlendorf, I. *J. Phys. Chem. B* **1999**, *103*, 692–698.
(18) Oekermann, T.; Yoshida, T.; Minoura, H.; Wijayantha, K. G. U.; Peter, L. M. *J. Phys. Chem. B* **2004**, *108*, 8364–8370.
(19) Manoj, A. G.; Alagiriswamy, A. A.; Narayan, K. S. *J. Appl. Phys.* **2003**, *94*, 4088–4095.
(20) Savenije, T. J.; Goossens, A. *Phys. Rev. B* **2001**, *64*, 115323.
(21) DiCarmine, P. M.; Semenikhin, O. A. *Electrochim. Acta* **2008**, *53*, 3744–3754.
(22) Daoud, W. A.; Turner, M. L. *React. Funct. Polym.* **2006**, *66*, 13–20.
(23) Savenije, T. J.; Warman, J. M.; Goossens, A. *Chem. Phys. Lett.* **1998**, *287*, 148–153.
(24) Breeze, A. J.; Schlesinger, Z.; Carter, S. A.; Brock, P. J. *Phys. Rev. B* **2001**, *64*, 125205.
(25) Arango, A. C.; Carter, S. A.; Brock, P. J. *Appl. Phys. Lett.* **1999**, *74*, 1698–1700.
(26) Gregg, B. A.; Hanna, M. C. *J. Appl. Phys.* **2003**, *93*, 3605–3614.
(27) Gregg, B. A. *J. Phys. Chem. B* **2003**, *107*, 4688–4698.
(28) Salafsky, J. S. *Phys. Rev. B* **1999**, *59*, 10885–10894.
(29) Watkins, P. K.; Walker, A. B.; Verschoor, G. L. B. *Nano Lett.* **2005**, *5*, 1814–1818.
(30) Yu, G.; Gao, J.; Hummelen, J. C.; Wudl, F.; Heeger, A. J. *Science* **1995**, *270*, 1789–1791.
(31) Halls, J. J. M.; Walsh, C. A.; Greenham, N. C.; Marseglia, E. A.; Friend, R. H.; Moratti, S. C.; Holmes, A. B. *Nature* **1995**, *376*, 498–500.
(32) Stübinger, T.; Brütting, W. *J. Appl. Phys.* **2001**, *90*, 3632–3641.
(33) Gregg, B. A.; Sprague, J.; Peterson, M. W. *J. Phys. Chem. B* **1997**, *101*, 5362–5369.
(34) Kroeze, J. E.; Savenije, T. J.; Vermeulen, M. J. W.; Warman, J. M. *J. Phys. Chem. B* **2003**, *107*, 7696–7705.
(35) Désormeaux, A.; Max, J. J.; Leblanc, R. M. *J. Phys. Chem.* **1993**, *97*, 6670–6678.
(36) Harrison, M. G.; Grüner, J.; Spencer, G. C. W. *Phys. Rev. B* **1997**, *55*, 7831–7849.
(37) Ghosh, A. K.; Feng, T. *J. Appl. Phys.* **1978**, *49*, 5982–5989.
(38) Kentre, V. M.; Wong, Y. M. *Phys. Rev. B* **1980**, *22*, 5716–5722.
(39) Braun, C. L. *J. Chem. Phys.* **1984**, *80*, 4157–4161.
(40) Koster, L. J. A.; Smits, E. C. P.; Mihailetchi, V. D.; Blom, P. W. M. *Phys. Rev. B* **2005**, *72*, 085205.
(41) Blom, P. W. M.; Mihailetchi, V. D.; Koster, L. J. A.; Markov, D. E. *Adv. Mater.* **2007**, *19*, 1551–1566.
(42) Kroeze, J. E.; Savenije, T. J.; Candeias, L. P.; Warman, J. M.; Siebbeles, L. D. A. *Sol. Energy Mater. Sol. Cells* **2005**, *85*, 189–203.
(43) Peumans, P.; Forrest, S. R. *Chem. Phys. Lett.* **2004**, *398*, 27–31.
(44) Umeda, M.; Nishizawa, M.; Itoh, T.; Selman, J. R.; Uchida, I. *Chem. Phys. Lett.* **2000**, *326*, 219–224.
(45) Kern, R.; Sastrawan, R.; Ferber, J.; Stangl, R.; Luther, J. *Electrochchim. Acta* **2002**, *47*, 4213–4225.
(46) Smilowitz, L.; Hays, A.; Heeger, A. J.; Wang, G.; Bowers, J. E. *J. Chem. Phys.* **1993**, *98*, 6504–6509.
(47) Schlichthörl, G.; Huang, S. Y.; Sprague, J.; Frank, A. J. *J. Phys. Chem. B* **1997**, *101*, 8141–8155.
(48) Goodman, A. M.; Rose, A. *J. Appl. Phys.* **1971**, *42*, 2823–2830.
(49) Mihailetchi, V. D.; Wildeman, J.; Blom, P.W. M. *Phys. Rev. Lett.* **2005**, *94*, 126602.
(50) Koehler, M.; Roman, L. S.; Inganäs, O.; da Luz, M. G. E. *J. Appl. Phys.* **2004**, *96*, 40–43.

JP8032512